Optimization of Multi-Section and Partially Augmented Magnetic Resonance Imaging (MRI) Images for Brain Tumor Classification Using ResNet-50

I Gede Susrama Mas Diyasa[1*], Victor Immanuel Sunarko[2], Eva Yulia Puspaningrum[3], Vaizal Asy'ari[4], and Mohd Zamri Ibrahim[5]
[1,4]Department of Information Technology, Faculty of Computer Science,
Universitas Pembangunan Nasional 'Veteran' Jawa Timur
Jawa Timur, Indonesia 60294
[2,3]Department of Informatics, Faculty of Computer Science,
Universitas Pembangunan Nasional 'Veteran' Jawa Timur
Jawa Timur, Indonesia 60294
[5]Faculty of Electrical and Electronics Engineering Technology,
Universiti Malaysia Pahang Al-Sultan Abdullah
Pahang, Malaysia 26600
Email: [1]igsusrama.if@upnjatim.ac.id, [2]21081010145@student.upnjatim.ac.id,
[3]evapuspaningrum.if@upnjatim.ac.id, [4]vaiz.asyari@gmail.com, [5]zamri@umpsa.edu.my

***Abstract*—Brain tumor diagnosis is challenging due to complex brain anatomy and tumor variability across imaging views. Traditional methods are manual and error-prone, making deep learning, particularly ResNet-based Convolutional Neural Network (CNN), essential for improving accuracy. The research investigates the enhancement of brain tumor classification using Magnetic Resonance Imaging (MRI) images through a novel modification of the ResNet50 model. It specifically addresses data imbalance challenges in medical image analysis. By proposing a targeted approach to partial data augmentation, the researchers aim to overcome limitations in traditional deep-learning classification methodologies, particularly the performance bottlenecks encountered in differentiating complex brain tumor subtypes. The research uses MRI dataset containing 5,249 labeled images (glioma, meningioma, pituitary, no tumor) across axial, coronal, and sagittal planes, highlighting class and view-based imbalances addressed through targeted augmentation. The research employs transfer learning to analyze three scenarios: non-augmented, partially augmented, and rounding-down data. Results reveal that the partially augmented scenario achieves the highest classification accuracy at 85%, significantly surpassing the non-augmented scenario, which peaks at 79%. In contrast, the rounding-down scenario yields only 60.16% accuracy during validation, highlighting the negative impact of drastically reducing data quantities. The unique contribution lies in demonstrating how strategic partial augmentation can enhance pattern recognition and mitigate overfitting risks, particularly in medical imaging where precise differentiation is crucial. The findings highlight the critical role of nuanced data distribution in enhancing model robustness, as evidenced by improved pattern recognition and reduced overfitting risks in the augmented scenario.**

***Index Terms*—Magnetic Resonance Imaging (MRI), Brain Tumor, ResNet-50**

I. Introduction

BRAIN tumors occur when cells or tissues grow abnormally in the brain area. In Indonesia, brain tumor cases are considered rare compared to other types of tumors, such as breast cancer. According to GCO data from 2022, there were four brain tumor cases per 100,000 inhabitants, a relatively low figure compared to breast cancer cases, which stood at 41.8 per 100,000 inhabitants [1]. However, the location of these abnormal cells makes brain tumors particularly dangerous. The brain functions as the control center of the human body, so abnormality in this area can lead to severe and extensive complications, such as swelling and pressure on blood vessels. Given the life-threatening nature of brain tumors, if not addressed

Received: Oct. 31, 2024; received in revised form: Feb. 01, 2025; accepted: Feb. 03, 2025; available online: May 05, 2025.
*Corresponding Author

promptly, it is crucial for medical experts to make swift and accurate decisions.

The diagnosis of brain tumors typically relies on images from Magnetic Resonance Imaging (MRI) equipment. It is due to MRI's ability to provide detailed images that highlight brain structures more effectively than CT scans or ultrasounds [2]. MRI imaging creates contrast in brain fibers, making it easier to distinguish between solid structures and tumors. Additionally, MRI scans of brain tumors can be viewed in three different planes: axial, coronal, and sagittal. The axial plane divides the brain into top and bottom sections [3]. Then, the coronal plane separates it from front to back, and the sagittal plane divides it parallel to the body's midline, from left to right. This variety of perspectives enhances the visualization of important features in both normal and tumorous brain structures.

The brain's complex structure and the variety of potential brain conditions make accurate diagnosis a time-consuming task for medical teams [4]. As technology advances, improving the speed and accuracy of diagnoses becomes increasingly important, especially since traditional methods for diagnosing brain tumors are predominantly manual. One promising approach to enhance both the speed and accuracy of diagnosis is the use of Artificial Intelligence (AI) [5].

AI has become an integral part of daily life, particularly in healthcare. In the medical field, it is commonly used to support decision-making and image analysis. AI helps to provide valuable information, including treatment recommendations, options, and additional insights [6]. Recent studies indicate that AI systems and AI-based applications are increasingly applied to enhance the professional medical environment [7]. It is crucial to apply AI techniques, particularly in the field of computer vision, to improve the speed and accuracy of brain tumor diagnosis [8]. Computer vision plays a vital role in assisting with brain tumor diagnosis by identifying objects and even individuals within images [9]. Computers can interpret contextual information from image data based on specific patterns extracted directly from the images, utilizing methods from computer vision.

One of the most commonly used methods in image recognition is the Convolutional Neural Network (CNN) [10, 11], which is a popular architecture for image classification. The convolutional layers effectively highlight essential features, such as the edges and textures of an object, allowing machines to recognize the object's unique identity more accurately. However, a primary limitation of the CNN architecture is its complexity. When developers try to increase the model's complexity, they may encounter the vanishing gradient problem, where key image features can be lost due to the pooling layers in the CNN structure.

The research is based on previous studies that provide references and guidelines. The review highlights numerous studies focused on utilizing CNN for brain tumor classification, often employing similar data class divisions. First, CNN is used as the foundation for the multi-class classification of brain tumors. The previous research has optimized CNN architecture by integrating three classification processes within a single AI model. It utilizes data from four datasets, totaling approximately 11,500 brain MRI images, and achieves exceptional performance: 99.33% accuracy for the first layer classification, 92.66% for the second layer, and 98.14% for the third layer. It demonstrates the potential of CNN to handle high complexity with substantial training data. However, it is limited to axial brain MRI images, which result in uniformity in the extracted tumor features [12].

Second, CNN architecture is utilized to classify brain tumors, demonstrating its effectiveness in diagnosing brain tumors through MRI analysis. The previous research has achieved a classification accuracy of 98.677% in identifying tumor types such as ependymoma, meningioma, and medulloblastoma. It emphasizes the importance of optimizing the number of training epochs, as increasing the epochs from 1 to 15 significantly improves the system's accuracy and sensitivity. However, challenges such as overfitting and dependence on dataset quality persist, highlighting the need for a careful approach to developing classification models [13].

Third, previous research also demonstrates the potential of ResNet50 in brain tumor classification, particularly emphasizing the challenges of low-resolution MRI images. It explores super-resolution techniques using Discrete Cosine Transform (DCT) and CNN, achieving 98.14% accuracy in tumor classification [14]. However, it does not extensively address data augmentation strategies or the impact of partial image augmentation, which becomes the primary motivation for the current research in optimizing multi-section MRI image classification using ResNet-50. The research aims to build upon these foundational approaches to improve classification accuracy and model robustness in brain tumor detection by focusing on strategic data augmentation and transfer learning.

Fourth, previous research [15] has employed the ResNet-152 architecture for classifying brain tumors. The model achieves an impressive 99% training accuracy, but its validation accuracy is only 81%. This significant discrepancy between training and validation accuracy hints at a potential overfitting issue, likely due to the failure to differentiate between sectional brain planes during the training process.

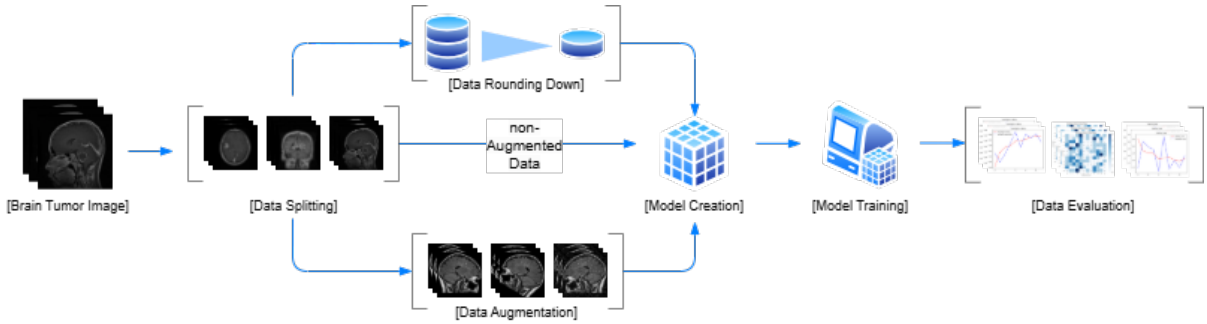

Fig. 1. Block diagram.

Fifth, previous research [16] has utilized ResNet-152 with the Chimp Optimizer to classify brain tumors, focusing specifically on axial plane images. This approach achieves a training accuracy of 98.85% and a validation accuracy of 97.64%. It effectively reduces the training and validation accuracy gap by concentrating on a specific brain plane for data selection.

The previous studies collectively indicate that relying solely on CNN architecture may not yield significant results in brain tumor classification [17]. Residual Networks (ResNet) provide a potential solution for improving accuracy [18, 19]. However, they demand substantial amounts of data. As MRI data undergoes various preprocessing techniques, such as separating sectional planes, the research focusing on this segmentation shows robust and high accuracy [2].

The ResNet is designed to tackle the vanishing gradient problem by utilizing a residual block architecture that preserves important image features. It includes connections that allow neurons with intact gradients to bypass certain processing layers, later combining with neurons that have undergone deeper processing [20]. The residual blocks within the ResNet architecture help to maintain the integrity of the image data throughout the processing stages.

Data separation based on sectional planes is crucial for improving the performance of the proposed ResNet model [12]. By keeping the sectional planes distinct, the model preserves specific information and unique patterns associated with each plane, preventing them from merging. This separation enables the model to more accurately identify brain tumors by recognizing distinct and unmixed patterns.

ResNet-50 is selected as a foundational experimental architecture to explore brain tumor classification due to its simplicity and proven effectiveness in deep learning image recognition tasks [13, 19, 21, 22]. As the most basic variant in the ResNet family, it provides a standard baseline model with 50 layers that demonstrate the core principles of residual learning, skip connections, and feature hierarchy optimization. This choice allows researchers to establish a fundamental understanding of how deep convolutional neural networks can be adapted for medical image analysis, serving as a critical starting point for more complex model developments in brain tumor classification. However, challenges persist in handling limited or imbalanced medical imaging datasets. Hence, the research proposes a novel partial augmentation approach to address data distribution challenges in brain tumor classification.

II. Research Method

As research progresses, a block diagram is developed to keep the research focused on its primary objective. This diagram provides a functional overview of the research workflow, illustrating how each element is interconnected. This structured approach helps to maintain clarity and alignment with the research goals.

The block diagram in Fig. 1 illustrates the initial step of data acquisition, specifically focusing on MRI images of brain tumors. After acquiring the data, it is categorized according to the perspective of each MRI image. Once processed, the data are input into a classification model under various scenarios, and its accuracy and robustness are evaluated.

A. Data Acquisition

The data collection process starts with a review of previous studies to identify the appropriate type of data for analysis. The researchers select brain tumor classification data that utilize MRI images. The data are from Kaggle, specifically from the dataset titled "*MRI for Brain Tumor with Bounding Boxes*".

The collected data consists of secondary data, comprising 5,249 training images in ".jpg" format, categorized as shown in Table I. This dataset includes MRI brain scan images classified into four categories: Glioma, Meningioma, Pituitary, and No Tumor. Each category contains a different number of training and

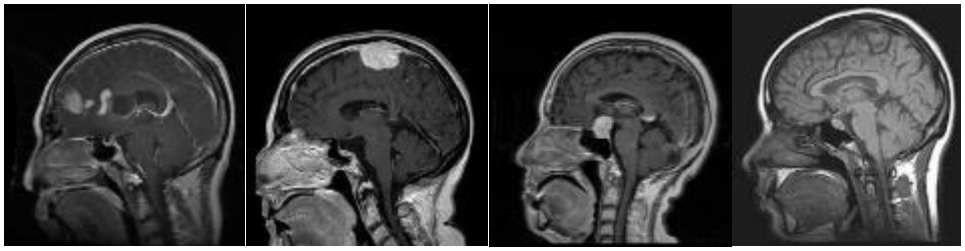

Fig. 2. Brain tumor sample data.

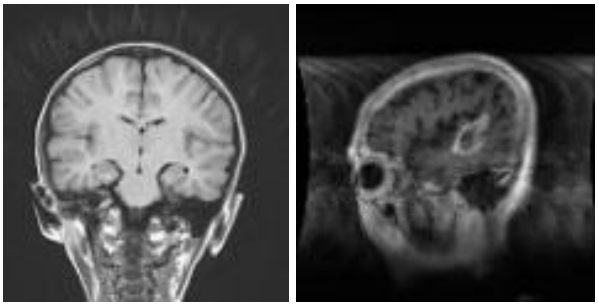

Fig. 3. Data with noise.

TABLE I
BRAIN TUMOR DATA.

No	Category	Training Data	Validation Data
1	Glioma	1,153	136
2	Meningioma	1,449	140
3	Pituitary	1,424	136
4	No Tumor	711	100
Total		4,737	512

validation images, with a total of 4,737 training and 512 validation samples. The data distribution reflects class imbalance, which may influence model performance and should be addressed during preprocessing or training. These images serve as the input for developing and evaluating machine learning models for brain tumor classification.

Figure 2 shows a sample of the data used. The images are labeled as glioma, meningioma, pituitary, and no tumor from left to right. The data are preprocessed for the subsequent stages. The primary research limitation stems from its reliance on the Kaggle brain tumor dataset, which, while comprehensive, may not fully represent the entire spectrum of brain tumor imaging variations encountered in clinical settings. The dataset's potential biases include limited demographic diversity, potential selection bias in image acquisition, and a restricted range of tumor types and stages. While Kaggle datasets provide a standardized platform for research, they often lack the complex heterogeneity found in real-world medical imaging. The dataset's controlled nature means that the model's performance may not directly translate to more diverse and challenging clinical scenarios, where imaging conditions, equipment variations, and patient-specific factors can significantly impact image quality and tumor characteristics.

B. Data Cleaning

The acquired data undergo a manual cleaning process. Images with considerable noise or artifacts may interfere with feature extraction in the model [21, 22], so they are removed to ensure optimal performance in later stages. In Fig. 3, MRI images of brain tumors often show distinct shadow lines surrounding the brain. These elements, aside from the actual brain, can greatly influence the pattern recognition process. As a result, it is essential to include a data removal step to eliminate any non-brain components.

C. Data Classification

The cleaned data also undergo a manual classification process. This process involves sorting the data from axial, coronal, and sagittal perspectives. Each perspective has its unique identifying features [23]. The axial view excels in providing a complete view of the brain hemispheres. Then, the coronal view displays the entire head from top to bottom in a single image from a perpendicular angle. In contrast, the sagittal view

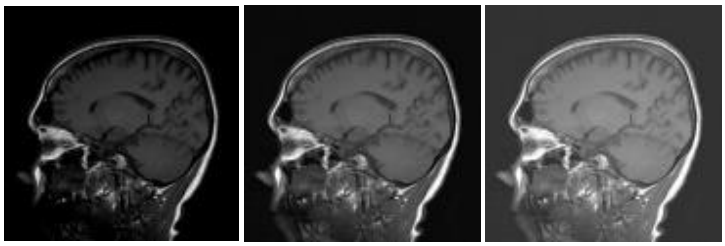

Fig. 4. Brightness manipulation result.

TABLE II
CLASSIFIED BRAIN TUMOR DATA.

No	Category	Plane	Training Data	Validation Data
1	Glioma	Axial	362	61
		Coronal	426	39
		Sagittal	365	36
2	Meningioma	Axial	389	62
		Coronal	508	48
		Sagittal	550	30
3	Pituitary	Axial	431	53
		Coronal	475	37
		Sagittal	518	46
4	No Tumor	Axial	617	80
		Coronal	38	11
		Sagittal	56	9
Total			4,735	512

presents the entire head from top to bottom in a single image parallel to the body's midline.

The results of the manual classification can be seen in Table II. It presents a classification of the brain tumor dataset according to the imaging planes of axial, coronal, and sagittal across each tumor category. The distribution highlights a substantial imbalance, both inter-class and intra-class, particularly evident in the no tumor category and within specific imaging planes such as coronal and sagittal. Such heterogeneity in data distribution may adversely affect the model's learning process, potentially leading to biased predictions. Consequently, it is imperative to implement data augmentation or balancing strategies to ensure equitable representation and enhance the model's generalization capabilities.

D. Data Augmentation

Data augmentation in the field of imaging involves manipulating the pixel values of an image. By applying augmentation techniques to the limited dataset, it is possible to enrich the variety of the available data [24, 25]. Machines interpret image data by analyzing the values of each pixel, meaning that even a single pixel difference can categorize the data as distinct from others [26]. Thus, data augmentation can serve as a solution to address issues related to data scarcity or overfitting during model training [27, 28]. The data augmentation methods utilized include brightness adjustment, darkening, horizontal flipping, rotation, and the addition of salt-and-pepper noise. As shown in Eq. (1), brightness adjustment involves manipulating pixel values by increasing or decreasing each pixel's scalar value. Increasing the value of each pixel in the image enhances its brightness. Conversely, decreasing the value of each pixel reduces the image's brightness.

$$f(x,y)^{'} = f(x,y) \pm b. \tag{1}$$

Equation (1) defines a basic brightness adjustment operation, where $f(x,y)^{'}$ represents the new pixel value at position (x,y), and $f(x,y)$ denotes the original pixel value. The term $\pm b$ corresponds to a constant scalar value added to or subtracted from each pixel. A positive value of b increases the pixel intensity, resulting in a brighter image, while a negative value of b decreases the pixel intensity, producing a darker image. This operation is applied uniformly across all pixels in the image.

Figure 4 demonstrates how brightness adjustment affects image visibility and contrast. Darkening reduces the visibility of fine details, which may be useful in simulating low-light conditions or testing model robustness. In contrast, brightness enhancement can highlight subtle structures, aiding in feature extraction and visual interpretation. Such transformations are essential in data augmentation strategies to improve model generalization across varying lighting conditions.

As shown in Eq. (2), horizontal flipping involves manipulating pixel values by mirroring the original image horizontally. Pixels that are originally on the left side of the image are translated to the right side, and vice versa. Equation (2) represents the horizontal flipping operation, where $f(x,y)^{'}$ is the transformed pixel value at position (x,y), and $f(N-x,y)$ denotes the corresponding pixel value from the original image. Here, N represents the image width minus one, effectively reversing the horizontal position of each pixel. This transformation mirrors the image along

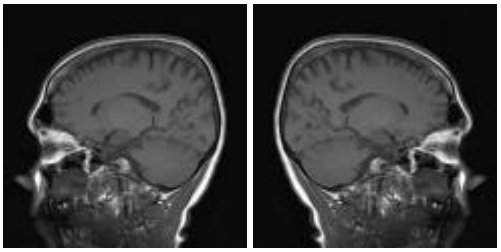

Fig. 5. Horizontal flip result.

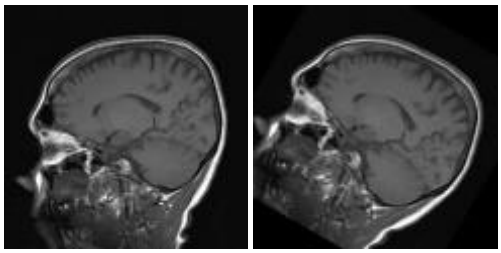

Fig. 6. Rotation result.

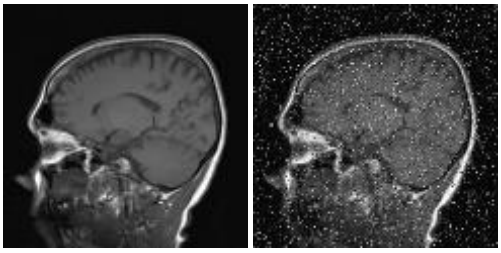

Fig. 7. Salt and pepper result.

the vertical axis, swapping pixel positions from left to right. Horizontal flipping is commonly used in data augmentation to introduce spatial variation and improve the robustness of machine learning models.

$$f(x,y)^{'} = f(N-x,y). \tag{2}$$

In Fig. 5, the image on the left is the normal image. Meanwhile, the image on the right is the result of the horizontal flip. The horizontal flip alters the pixel arrangement, resulting in a different sequence of pixels across the image. This transformation is particularly useful in data augmentation, as it introduces spatial diversity without altering the semantic content of the image. By reversing the horizontal orientation, models can be trained to recognize features regardless of their left-right positioning, enhancing their generalization capabilities. Such augmentation is especially beneficial in medical imaging, where anatomical structures may appear in varying orientations.

As shown in Eq. (3), rotation is a process of manipulating image data by changing its orientation around the center point of the image. This transformation can be accomplished by applying trigonometric formulas to each pixel. This results in new pixel positions being calculated based on the specified rotation angle.

$$f(x,y)^{'} = f(x\cos\Theta - y\sin\Theta, x\sin\Theta + y\cos\Theta). \tag{3}$$

In Fig. 6, the image on the left is the normal image. Meanwhile, the image on the right shows the result of the rotation. The image maintains the same dimensions, but the position of each pixel is translated relative to the center point of the image by an angle of 45 degrees in a clockwise direction. This rotation technique is widely applied in data augmentation to enhance model invariance to orientation changes. By rotating the image around its center, spatial relationships between anatomical structures are preserved while introducing geometric diversity. Such transformations help to improve the robustness and generalization of deep learning models in medical image analysis.

Lastly, salt and pepper is a process of manipulating pixel values by adding noise to the image data. Salt and pepper noise is a type of noise that appears as sharp disturbances in the image, manifested as randomly scattered black and/or white spots throughout the image [29]. In Fig. 7, the image on the left is the normal image, while the image on the right illustrates the result of the salt and pepper noise. The image affected by this noise will display dark pixels in bright areas and bright pixels in dark areas. This noise can be caused by several factors, such as dead pixels, errors in the analog-to-digital conversion process, or bit errors during transmission.

E. Proposed Model

The model used is a result of transfer learning from ResNet50, sourced from the TensorFlow library. The ResNet architecture consists of several residual blocks. In general, this approach employs a technique known as skip connection [30]. The skip connection links the activations of one layer to subsequent layers by bypassing some layers in between. This arrangement creates a residual block. ResNets are constructed by stacking these residual blocks together. As seen in Eq. (4), the residual block allows a neuron to be processed through convolutional layers while maintaining its gradient before processing. It enables neurons that have previously experienced vanishing gradients to regain the gradients that are characteristic of the data being processed.

$$F(x) := H(x) - x, \text{gives } H(x) := F(x) + x. \tag{4}$$

TABLE III
COMPILATIONS OF MODEL PARAMETERS.

No	Parameter	Value
1	Optimizer	Adam
2	Loss	Categorical Crossentropy
3	Evaluation	Accuracy
4	Epochs	25
5	Batch Size	16

TABLE IV
PARTIALLY AUGMENTED DATA.

No	Category	Plane	Training Data	Validation Data
1	Glioma	Axial	362	61
		Coronal	426	39
		Sagittal	365	36
2	Meningioma	Axial	389	62
		Coronal	508	48
		Sagittal	550	30
3	Pituitary	Axial	431	53
		Coronal	475	37
		Sagittal	518	46
4	No Tumor	Axial	617	80
		Coronal	204	11
		Sagittal	546	9
Total			5,391	512

As shown in Eq. (4), the residual block is designed to reformulate the learning process by allowing the network to approximate the residual function $F(x) := H(x) - x$, rather than learning the direct mapping $H(x)$. In this context, x represents the input to the residual block, $H(x)$ is the target underlying mapping to be learned, and $F(x)$ denotes the residual function that captures the difference between the desired output and the input. By rearranging the equation as $H(x) := F(x) + x$, the network effectively adds the learned residual back to the original input. This structure maintains the flow of gradients during backpropagation, thus addressing the vanishing gradient problem and enabling the successful training of deeper neural networks.

Given its advantages, ResNet has proven quite effective in image recognition or classification based on the properties of its residual blocks [30]. The residual blocks in the ResNet architecture enable image data to retain previously extracted features, allowing for deeper processing of the image data without the concern of losing those features during convolution or other processes. This capability supports the learning of more complex patterns, as the network can leverage both newly learned and previously preserved features simultaneously. Moreover, it enhances training efficiency and accuracy by enabling the construction of substantially deeper networks without degradation in performance.

Additionally, modifications are made by changing the softmax layer in the fully connected layer to accommodate 12 classes in accordance with the previous data distribution [31, 32]. The transfer learning model is configured with its trainable parameters set to false to avoid potential overfitting. Table III highlights the essential parameters used in constructing the ResNet50 model. A callback for early stopping is applied during training. The training halts if the training accuracy reaches 92% and validation accuracy reaches 90% or there is no improvement in validation accuracy within a patience of 5 epochs.

The proposed model is tested under multiple scenarios to assess its effectiveness using the research methodology gathered. Each scenario is evaluated by monitoring the training and validation accuracy and loss. The Adam optimizer is selected for its adaptive learning rate capabilities, which help to accelerate convergence during training. Categorical crossentropy is employed as the loss function due to the multi-class classification nature of the problem, while accuracy is used to evaluate model performance. The model is trained over 25 epochs with a batch size of 16, providing a balanced trade-off between computational efficiency and model generalization. The data details for the non-augmented testing scenario can be seen in Table III.

In Table IV, particularly in the coronal and sagittal rows, a significant increase in data can be observed. Data augmentation is performed partially, targeting the classes with the smallest percentage of samples to enhance their quantity, thereby reducing the gap between their amounts and those of the other classes. This approach ensures a more balanced dataset, facilitating improved model training and classification performance.

In Table V, a significant portion of the data is trimmed to match the quantity with that of the class with the smallest number of samples. This normalization process ensures a balanced training dataset and helps prevent the model from becoming biased toward classes with larger sample sizes. Although validation data remains unchanged to preserve evaluation integrity, the training data are equalized to enhance fairness during model learning. This method is particularly beneficial in scenarios involving class imbalance in medical imaging datasets. Moreover, it provides a controlled environment to evaluate the model's capacity to learn from uniformly distributed data, highlighting its core classification ability without bias from data volume.

These three scenarios are trained using the ResNet50 model with the compilation settings detailed in Table III. Each model presents unique characteristics throughout the training process due to variations in data

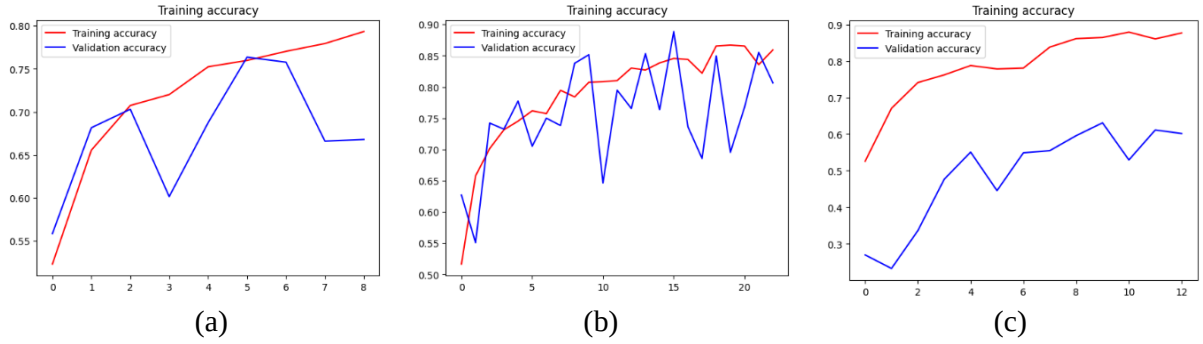

Fig. 8. The accuracy of models.

TABLE V
ROUNDING-DOWN DATA.

No	Category	Plane	Training Data	Validation Data
1	Glioma	Axial	38	61
		Coronal	38	39
		Sagittal	38	36
2	Meningioma	Axial	38	62
		Coronal	38	48
		Sagittal	38	30
3	Pituitary	Axial	38	53
		Coronal	38	37
		Sagittal	38	46
4	No Tumor	Axial	38	80
		Coronal	38	11
		Sagittal	38	9
Total			456	512

handling. It may influence performance metrics like accuracy and robustness across different test scenarios.

F. Evaluation Metrics

The trained model's performance is evaluated using accuracy derived from the confusion matrix, a table that provides a comprehensive assessment by comparing model predictions to actual labels. This matrix includes four main components: True Positive (TP), which represents instances correctly identified as positive; True Negative (TN), indicating instances accurately classified as negative; False Positive (FP), where instances are mistakenly classified as positive; and False Negative (FN), where instances are incorrectly classified as negative. Together, these elements offer a detailed view of the model's strengths and weaknesses, allowing for an analysis that goes beyond simple accuracy and reveals patterns in prediction errors. It helps to identify any tendencies the model may have toward overpredicting or underpredicting specific classes.

The specific metric extracted from the confusion matrix for evaluation is overall accuracy, calculated as shown in Eq. (5). It involves summing the total number of correct predictions–both TP and TN–and dividing this by the total number of predictions made. This ratio provides a straightforward measure of the model's general classification accuracy, offering insight into how effectively the model is distinguishing between classes across the dataset.

$$\frac{TP + TN}{(TF + TN + FP + FN)}. \tag{5}$$

III. RESULTS AND DISCUSSION

The research results are derived from training each model under various scenarios. Each training session uses a single data source: secondary data collected from the Kaggle website. This standardized data source ensures consistent input quality across all model scenarios, facilitating a clear comparison of each model's performance in different experimental settings.

Figure 8 illustrates the different outcomes for each training scenario. Figure 8(a) shows the training histories for models using non-augmented data. Then, Fig. 8(b) shows the training histories using data with partial augmentation. Figure 8(c) presents the training histories using data that has been balanced through down-sampling to match the smallest class size. These variations in training histories demonstrate how each data-handling approach affects model performance across the different scenarios.

The model trained with non-augmented data achieves a lower maximum accuracy compared to the model trained with augmented data. According to the accuracy history graph, the augmented data model reaches a peak accuracy of 85%, whereas the non-augmented model only achieves a peak accuracy of 79%. This result suggests that augmenting data significantly improves the model's performance, likely due to the enhanced variability and robustness provided by the additional augmented samples.

Table II highlights the noticeable data imbalance in this study, particularly in the "no tumor" class within

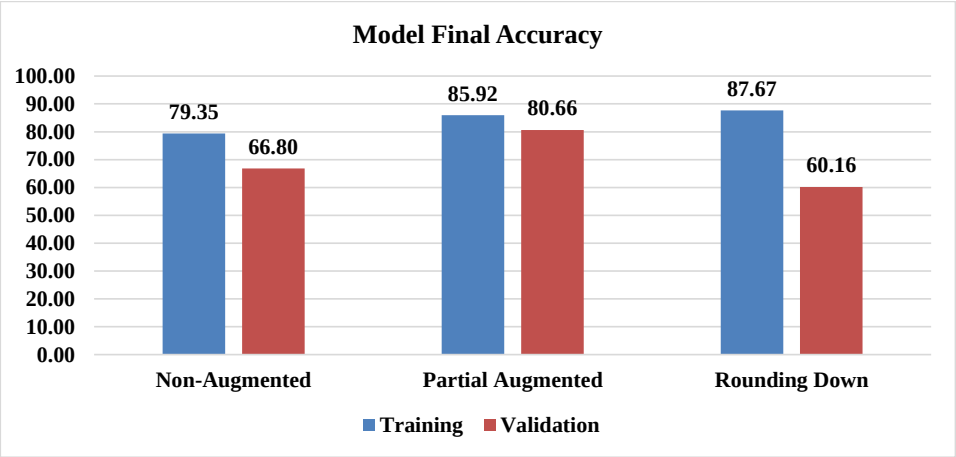

Fig. 9. Final accuracy of the models.

coronal and sagittal views. This imbalance is likely to hinder the model's ability to perform optimally in classifying all twelve classes, thus necessitating data augmentation. The training history in Fig. 8 shows that even when augmentation is applied, it only partially addresses data gaps. It does not negatively impact model training. On the contrary, adding augmented data enhances the model's performance, yielding a higher accuracy history compared to the non-augmented data scenario.

In terms of model robustness, the first and second training scenarios exhibit only a slight difference between training and validation accuracy, suggesting that the model generalizes well when recognizing unseen data. It also demonstrates the positive impact of data augmentation in replicating image data. Even with basic image processing techniques, the augmented data retains significant features comparable to those of diverse, original data, contributing to model stability and reliable performance.

In contrast, the model trained with down-sampled data exhibits severe underfitting. While the accuracy history indicates some growth, there is a significant gap between training and validation accuracy. This model achieves a final accuracy of 87.67% on the training set but only 60.16% on the validation set. The over 25% difference suggests that the model lacks generalizability for new data. Although it performs well in terms of training accuracy, it fails to deliver similar results during validation, highlighting its limitations in recognizing unfamiliar patterns.

From the final results in Fig. 9, the model trained with partially augmented data demonstrates superior overall accuracy compared to the other scenarios. Specifically, the partially augmented data model achieves higher accuracy than the non-augmented data model, despite the significant data imbalance. This outcome substantiates that even partial data augmentation effectively reduces the impact of data imbalance and significantly enhances the model's classification accuracy. Interestingly, the model using the rounding-down scenario excels in its training process. This scenario achieves the highest training accuracy compared to other scenarios. This finding also demonstrates that balanced data distribution plays a critical role in the training process, even if the total quantity of data is limited. However, despite the model's impressive training performance, the reduced data quantity in this scenario leads to underfitting, as it struggles to generalize to new data effectively.

As shown in Fig. 10, the loss history for each scenario reveals some fluctuation. Figure 10(a) displays loss history for non-augmented data. Figure 10(b) shows partially augmented data. Figure 10(c) presents rounding-down data. The visible fluctuations suggest that the model may still be prone to overfitting. This observation presents an opportunity for further research to explore techniques to enhance the model's stability and robustness, potentially improving its generalization capabilities on unseen data.

Table VI is the corresponding label used in the confusion matrix evaluation. Each confusion matrix provides insights into the model's classification performance, highlighting areas of strength and weakness in accurately predicting the various classes. The patterns observed in these matrices are crucial for understanding the effectiveness of data augmentation and its impact on classification accuracy across different training scenarios.

In Fig. 11, lower accuracy rates and a higher in-

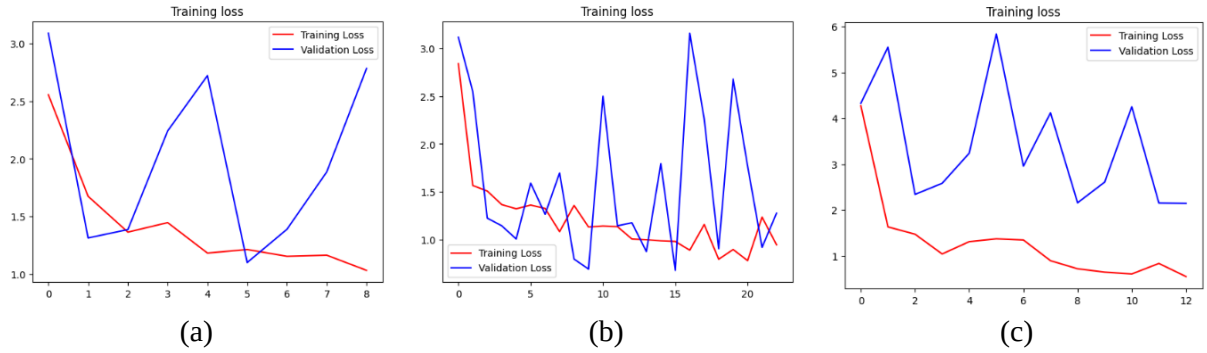

Fig. 10. Models' loss.

TABLE VI
CONFUSION MATRIX LABEL.

Label	Class
0	clear-axial
1	clear-coronal
2	clear-sagittal
3	glioma-axial
4	glioma-coronal
5	glioma-sagittal
6	meningioma-axial
7	meningioma-coronal
8	meningioma-sagittal
9	pituitary-axial
10	pituitary-coronal
11	pituitary-sagittal

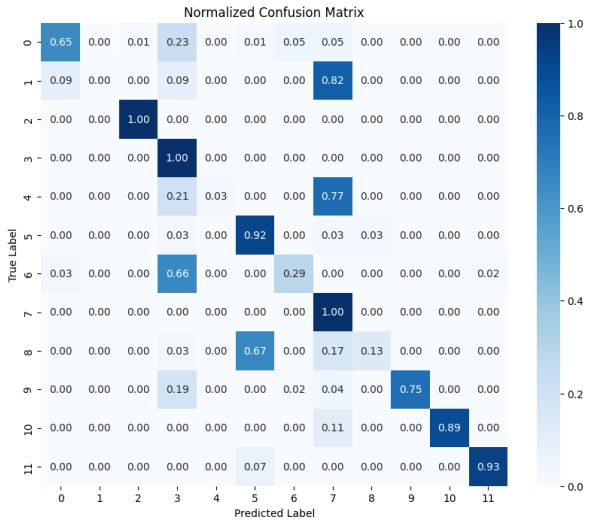

Fig. 11. Confusion matrix of normal data.

cidence of misclassification are evident in scenarios where significant data imbalance exists, such as in the clear-sagittal (2) and clear-coronal (1) classes. These classes are frequently misclassified as other tumor classes, such as glioma and meningioma, particularly when viewed from the same perspective. This is a fundamental issue in medical image classification when dealing with imbalanced datasets. The frequent misclassification suggests that the model struggles to identify distinctive features in these perspectives (clear-sagittal (2) and clear-coronal (1) classes). This limitation stems not only from the data scarcity but also from the inherent complexity of brain tumor morphology when viewed from different angles. The model's difficulty in establishing reliable patterns for clear classes demonstrates how critical data quantity and quality are in developing robust classification systems for medical imaging applications.

In Fig. 12, misclassification rates for the clear classes show a slight decline in the partial augmentation scenario. However, significant misclassification between views for tumor classes persists. While augmentation aids in enhancing the representation of clear classes, its impact remains limited when it comes to distinguishing clear classes from certain tumor classes. The persistent confusion between tumor types, particularly in sagittal views (e.g., meningioma-sagittal (8) and glioma-sagittal (5)), indicates that augmentation alone cannot fully address the challenges of view-dependent classification. This result suggests that the similarity in tumor appearance from certain angles presents a fundamental challenge that requires more sophisticated approaches beyond basic data augmentation techniques. The findings highlight the need for augmentation strategies that specifically target view-dependent features while preserving the distinct characteristics of different tumor types.

Lastly, in the rounding-down data scenario, the model exhibits lower accuracy and a more widespread misclassification, particularly within the clear and tumor classes sharing the same view. Based on Fig. 13, the reduction in data alleviates some of the imbalance issues. However, it also diminishes the model's ability to recognize the unique features of each class,

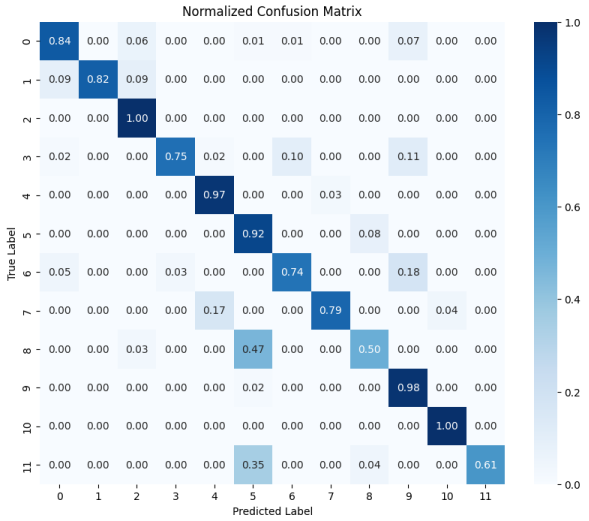

Fig. 12. Confusion matrix of partial augmented data.

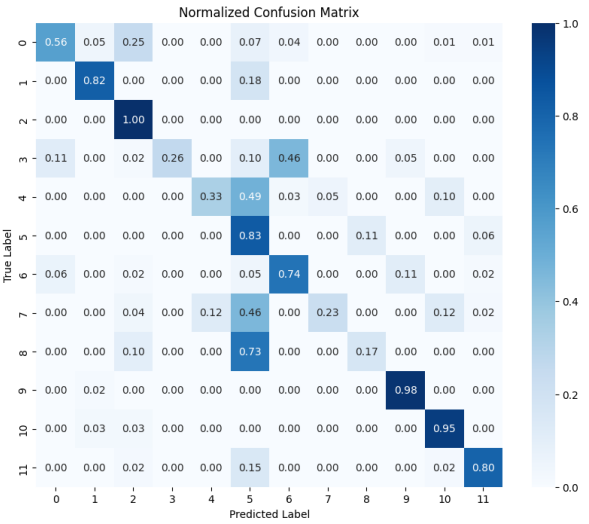

Fig. 13. Confusion matrix of rounding-down data.

especially in challenging views that are difficult to differentiate. The increase in misclassification among identical views (axial, coronal, and sagittal) highlights that the drastic reduction of data has detrimental effects on the model's performance, leading to confusion among different tumor types in the sagittal view. The findings emphasize that while addressing data imbalance is important, methods that drastically reduce data availability can undermine the model's capacity to develop robust classification capabilities.

Through a comprehensive evaluation of all three scenarios, the research reveals critical insights into the optimization of ResNet-50 for brain tumor classification using multi-section MRI images. The partial augmentation approach, achieving 85% accuracy, demonstrates the most promising balance between data enhancement and model performance. However, the persistent challenges in distinguishing between certain views and tumor types highlight the need for more sophisticated approaches.

Comparative analysis across scenarios emphasizes that while data quantity is crucial, the quality and distribution of training data play equally vital roles in model performance. These findings suggest that future developments should focus on targeted augmentation strategies that specifically address view-dependent features while maintaining the distinct characteristics necessary for accurate tumor classification. The results also underscore the importance of preserving sufficient data quantity while addressing class imbalance, as evidenced by the significant performance degradation in the rounding-down scenario. This comprehensive understanding provides valuable guidance for developing more effective approaches to medical image classification, particularly in scenarios where multiple viewing angles and tumor types must be accurately distinguished.

The overall accuracy calculation from the confusion matrix results can be detailed in Fig. 14. It illustrates the performance of the model across various scenarios, highlighting the differences in accuracy among the training methods employed. The analysis provides insights into how each scenario affects the model's ability to accurately classify the MRI brain tumor images, informing future improvements and adjustments to the methodology. Through Fig. 14, it is evident that the model excels in the partially augmented testing scenario. It aligns with the model's performance recorded in the history of accuracy and loss, which also demonstrates superior results compared to the other testing scenarios. The partial augmentation effectively enhances the model's ability to learn from the training data, resulting in improved classification outcomes and reduced misclassification rates.

IV. Conclusion

The researchers demonstrate that brain tumor classification using the multi-section concept has a lower potential for overfitting compared to models without sectioning. The models developed based on various scenarios, including partial augmentation, exhibit varying performance levels, highlighting that partial augmentation significantly enhances the model's performance. This approach not only helps in mitigating overfitting but also contributes to more accurate and reliable classifications, showcasing the effectiveness of incorporating multi-sectional analysis in brain tumor classification tasks.

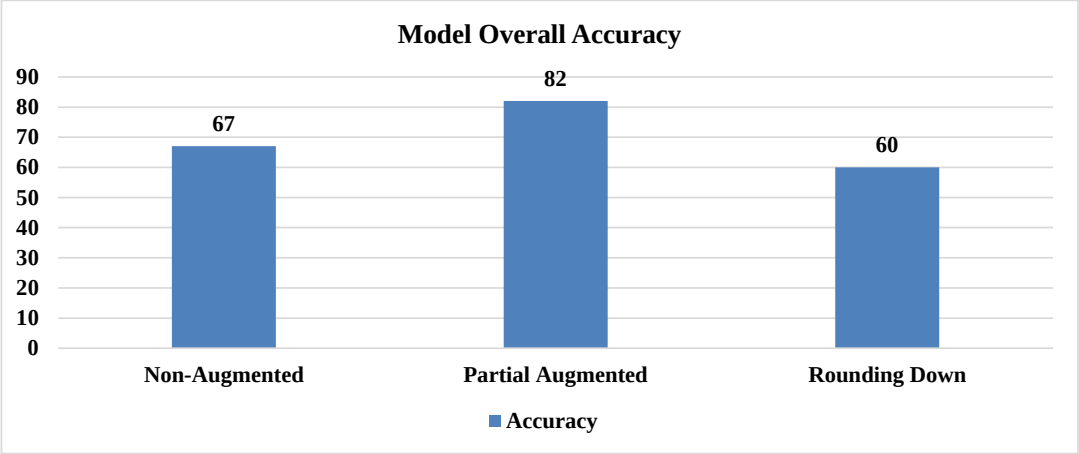

Fig. 14. Model's final accuracy.

Data distribution plays a crucial role in producing an effective model, as evidenced by the significant results observed in the rounding-down testing scenario during the training process. This finding underscores the importance of ensuring a balanced distribution of data quantities, which greatly influences the model's success in achieving high accuracy. A well-distributed dataset allows the model to learn more effectively from diverse examples, improving its ability to generalize and accurately classify different classes, ultimately leading to enhanced performance in real-world applications.

From the three scenarios conducted, partial data augmentation demonstrates limited improvement in addressing class imbalance but is insufficient to resolve the misclassification issues between clear and tumor classes within the same view. Meanwhile, the rounding-down scenario results in an overall decrease in accuracy. A more comprehensive augmentation strategy or the implementation of alternative balancing techniques may prove more effective in enhancing model accuracy, particularly for the clear class, and in distinguishing between challenging views, such as sagittal.

Overall, data plays a crucial role in the training process for classification using machine learning, particularly in the case of brain tumor classification using MRI images. Data with classes extended based on their viewpoints has proven to narrow the gap between training and validation accuracy, indicating that the model effectively recognizes the underlying patterns within the data. This scenario has successfully constructed a robust model.

One of the shortcomings identified in the research is the suboptimal accuracy across all testing scenarios, as the model fails to reach a significant accuracy level comparable to previous studies, which achieved over 90%. This limitation may stem from several factors, including imbalanced and insufficient additional data, particularly in the classes with severe discrepancies, such as coronal and sagittal views in the no-tumor category. Addressing these issues by enhancing data diversity and quantity can potentially improve the model's performance in future iterations.

Future research should focus on expanding the generalizability and robustness of the proposed ResNet-50 modification by integrating multi-institutional datasets that capture broader demographic and clinical variations. It will involve collaborating with diverse medical centers to create a more comprehensive dataset representing different imaging technologies, patient populations, and tumor subtypes. Researchers should explore advanced augmentation techniques such as Generative Adversarial Networks (GANs) for synthetic image generation, investigate transfer learning approaches across different imaging modalities, and develop more sophisticated techniques for handling class imbalance. Additionally, the research should aim to develop interpretable AI models that can provide clinically meaningful insights, enabling physicians to understand the decision-making process behind tumor classification and potentially uncovering subtle diagnostic patterns that may escape human perception.

Author Contribution

Conceived and designed the analysis, I. G. S. M. D.; Collected the data, I. G. S. M. D.; Contributed data or analysis tools, I. G. S. M. D.; Constructed and performed the model experiment, V. I. S.; Wrote the introduction and research method, V. I. S.; Created the

experiment design and environment, E. Y. P.; Wrote the research method and result, E. Y. P.; Performed the model experiment, V. A.; Wrote the experiment result, V. A. and M. Z. I.; and Gave advice about model performance and efficiency, M. Z. I.

Data Availability

The data that support the findings of the research are openly available in Kaggle at https://www.kaggle.com/datasets/ahmedsorour1/mri-for-brain-tumor-with-bounding-boxes?resource=download.

References

[1] Global Cancer Observatory, "Globocan 2022 statistics," 2022. [Online]. Available: https://gco.iarc.who.int/media/globocan/factsheets/populations/900-world-fact-sheet.pdf

[2] T. N. Papadomanolakis, E. S. Sergaki, A. A. Polydorou, A. G. Krasoudakis, G. N. Makris-Tsalikis, A. A. Polydorou, N. M. Afentakis, S. A. Athanasiou, I. O. Vardiambasis, and M. E. Zervakis, "Tumor diagnosis against other brain diseases using T2 MRI brain images and CNN binary classifier and DWT," *Brain Sciences*, vol. 13, no. 2, pp. 1–25, 2023.

[3] W. Tian, D. Li, M. Lv, and P. Huang, "Axial attention convolutional neural network for brain tumor segmentation with multi-modality MRI scans," *Brain Sciences*, vol. 13, no. 1, pp. 1–20, 2022.

[4] M. Arabahmadi, R. Farahbakhsh, and J. Rezazadeh, "Deep learning for smart healthcare—A survey on brain tumor detection from medical imaging," *Sensors*, vol. 22, no. 5, pp. 1–27, 2022.

[5] H. S. Basavegowda and G. Dagnew, "Deep learning approach for microarray cancer data classification," *CAAI Transactions on Intelligence Technology*, vol. 5, no. 1, pp. 22–33, 2020.

[6] H. Ayesha, S. Iqbal, M. Tariq, M. Abrar, M. Sanaullah, I. Abbas, A. Rehman, M. F. K. Niazi, and S. Hussain, "Automatic medical image interpretation: State of the art and future directions," *Pattern Recognition*, vol. 114, 2021.

[7] I. G. S. M. Diyasa, W. S. J. Saputra, A. A. N. Gunawan, D. Herawati, S. Munir, and S. Humairah, "Abnormality determination of spermatozoa motility using Gaussian mixture model and matching-based algorithm," *Journal of Robotics and Control (JRC)*, vol. 5, no. 1, pp. 103–116, 2024.

[8] R. Thangaraj, S. Anandamurugan, and V. K. Kaliappan, "Automated tomato leaf disease classification using transfer learning-based deep convolution neural network," *Journal of Plant Diseases and Protection*, vol. 128, no. 1, pp. 73–86, 2021.

[9] C. Janiesch, P. Zschech, and K. Heinrich, "Machine learning and deep learning," *Electronic Markets*, vol. 31, no. 3, pp. 685–695, 2021.

[10] W. Ayadi, W. Elhamzi, I. Charfi, and M. Atri, "Deep CNN for brain tumor classification," *Neural Processing Letters*, vol. 53, pp. 671–700, 2021.

[11] G. S. M. Diyasa, A. Fauzi, M. Idhom, and A. Setiawan, "Multi-face recognition for the detection of prisoners in jail using a modified cascade classifier and CNN," *Journal of Physics: Conference Series*, vol. 1844, pp. 1–10, 2021.

[12] E. Irmak, "Multi-classification of brain tumor MRI images using deep convolutional neural network with fully optimized framework," *Iranian Journal of Science and Technology, Transactions of Electrical Engineering*, vol. 45, no. 3, pp. 1015–1036, 2021.

[13] B. A. Mohammed and M. S. Al-Ani, "An efficient approach to diagnose brain tumors through deep CNN," *Mathematical Biosciences and Engineering*, vol. 18, no. 1, pp. 851–867, 2021.

[14] A. Deshpande, V. V. Estrela, and P. Patavardhan, "The DCT-CNN-ResNet50 architecture to classify brain tumors with super-resolution, convolutional neural network, and the ResNet50," *Neuroscience Informatics*, vol. 1, no. 4, pp. 1–8, 2021.

[15] A. Digdoyo, T. Surawan, A. S. B. Karno, D. R. Irawati, and Y. Effendi, "Deteksi dini tumor otak menggunakan metode deep learning arsitektur CNN Resnet-152," *Jurnal Teknologi*, vol. 9, no. 2, pp. 114–122, 2022.

[16] S. Athisayamani, R. S. Antonyswamy, V. Sarveshwaran, M. Almeshari, Y. Alzamil, and V. Ravi, "Feature extraction using a residual deep convolutional neural network (resnet-152) and optimized feature dimension reduction for MRI brain tumor classification," *Diagnostics*, vol. 13, no. 4, pp. 1–20, 2023.

[17] D. R. Nayak, N. Padhy, P. K. Mallick, M. Zymbler, and S. Kumar, "Brain tumor classification using dense Efficient-Net," *Axioms*, vol. 11, no. 1, pp. 1–13, 2022.

[18] G. Liang and L. Zheng, "A transfer learning method with deep residual network for pediatric pneumonia diagnosis," *Computer Methods and Programs in Biomedicine*, vol. 187, 2020.

[19] M. R. M. Ariefwan, I. G. S. M. Diyasa, and K. M. Hindrayani, "InceptionV3, ResNet50, ResNet18 and MobileNetV2 performance comparison on

face recognition classification," *Literasi Nusantara*, vol. 4, no. 1, pp. 1–10, 2023.

[20] S. Lu, S. H. Wang, and Y. D. Zhang, "Detecting pathological brain via ResNet and randomized neural networks," *Heliyon*, vol. 6, no. 12, pp. 1–11, 2020.

[21] A. S. Febrianti, T. A. Sardjono, and A. F. Babgei, "Klasifikasi tumor otak pada citra magnetic resonance image dengan menggunakan metode support vector machine," *Jurnal Teknik ITS*, vol. 9, no. 1, pp. A118–A123, 2020.

[22] G. Algan and I. Ulusoy, "Image classification with deep learning in the presence of noisy labels: A survey," *Knowledge-Based Systems*, vol. 215, 2021.

[23] L. H. Shehab, O. M. Fahmy, S. M. Gasser, and M. S. El-Mahallawy, "An efficient brain tumor image segmentation based on deep Residual Networks (ResNets)," *Journal of King Saud University-Engineering Sciences*, vol. 33, no. 6, pp. 404–412, 2021.

[24] Y. Anagun, "Smart brain tumor diagnosis system utilizing deep convolutional neural networks," *Multimedia Tools and Applications*, vol. 82, no. 28, pp. 44 527–44 553, 2023.

[25] A. R. Khan, S. Khan, M. Harouni, R. Abbasi, S. Iqbal, and Z. Mehmood, "Brain tumor segmentation using K-means clustering and deep learning with synthetic data augmentation for classification," *Microscopy Research and Technique*, vol. 84, no. 7, pp. 1389–1399, 2021.

[26] M. F. Alanazi, M. U. Ali, S. J. Hussain, A. Zafar, M. Mohatram, M. Irfan, R. AlRuwaili, M. Alruwaili, N. H. Ali, and A. M. Albarrak, "Brain tumor/mass classification framework using magnetic-resonance-imaging-based isolated and developed transfer deep-learning model," *Sensors*, vol. 22, no. 1, pp. 1–15, 2022.

[27] F. A. A. Harahap, A. N. Nafisa, E. N. D. B. Purba, and N. A. Putri, "Implementasi algoritma convolutional neural network arsitektur model MobileNetV2 dalam klasifikasi penyakit tumor otak glioma, pituitary dan meningioma," *Jurnal Teknologi Informasi, Komputer, dan Aplikasinya (JTIKA)*, vol. 5, no. 1, pp. 53–61, 2023.

[28] Q. Zheng, P. Zhao, Y. Li, H. Wang, and Y. Yang, "Spectrum interference-based two-level data augmentation method in deep learning for automatic modulation classification," *Neural Computing and Applications*, vol. 33, no. 13, pp. 7723–7745, 2021.

[29] C. Tian, L. Fei, W. Zheng, Y. Xu, W. Zuo, and C. W. Lin, "Deep learning on image denoising: An overview," *Neural Networks*, vol. 131, pp. 251–275, 2020.

[30] M. Shafiq and Z. Gu, "Deep residual learning for image recognition: A survey," *Applied sciences*, vol. 12, no. 18, pp. 1–43, 2022.

[31] F. Gao, B. Li, L. Chen, Z. Shang, X. Wei, and C. He, "A softmax classifier for high-precision classification of ultrasonic similar signals," *Ultrasonics*, vol. 112, 2021.

[32] S. Maharjan, A. Alsadoon, P. W. C. Prasad, T. Al-Dalain, and O. H. Alsadoon, "A novel enhanced softmax loss function for brain tumour detection using deep learning," *Journal of Neuroscience Methods*, vol. 330, 2020.